# DISCRETE ELEMENT MODELS OF A COHESIVE SOIL

**Rostislav CHOTEBORSKY[1], Jiří KURE[2], Egidijus KATINAS[2]**

[1]*Department of Material Science and Manufacturing Technology, Faculty of Engineering, Czech University of Life Sciences, Kamýcká 129, 165 21 Prague – Suchdol, Czech Republic*
[2]*Department of Electrical Engineering and Automation, Faculty of Engineering, Czech University of Life Sciences, Kamýcká 129, 165 21 Prague – Suchdol, Czech Republic*

***Abstract***
*The soil tensile test was performed to analyze the cohesive soil model. The results were obtained experimentally and from the simulation using the discrete element method with the new bond model suggested by the Rocky DEM software. The simulated tensile test results showed good agreement with the experimental results done in the laboratory. Thereafter, the effect of Young's modulus, normal stiffness, normal stress limit, tangential stiffness, and tangential stress limit was analyzed to generate maximal force, power, and stiffness during the simulation. As well as, multivariate equations were suggested to describe the influence of previously mentioned properties.*

***Key words:*** *soil; discrete element method; mechanical properties; cohesion.*

## INTRODUCTION

Tillage or non-tillage operations are carried out using mechanical energy, commonly using a tractor-drawn tool to achieve cutting, inversion, pulverization, and other types of soil movement. The energy required for soil processes accounts for a significant proportion of total energy used in crop production. With high fuel prices and increasing pressure on emissions, minimizing the energy used in crop production is essential. In soil processing, decreasing the draught forces and optimizing vertical forces are desired to reduce energy consumption. However, the experimental procedures involved have a high cost, and the extrapolation of the results to all conditions is uncertain (*Mattetti, Varani, Molari, & Morelli, 2017*). With the rapid development in computer technology, researchers have employed numerical methods to model the soil-tool interaction.

Numerical methods (*Mouazen & Neményi, 1999*), including the finite element method (FEM) and discrete element method (DEM), were also used to simulate the interaction between cohesionless soil and tillage tools (*Asaf, Rubinstein, & Shmulevich, 2007*). These methods could calculate tool forces and simulate soil loosening (*Mouazen & Neményi, 1999*). In DEM simulation, mixing and cracking propagation can be simulated. It is well-known that cohesive forces exist between soil particles, which are attributed to liquid bridges and living organisms with very complex behaviors (*Cundall & Hart, 1992*). Although these forces must be accounted in the DEM simulations, a few reports about this point can be found in the literature on soil–tool interaction, where is presented chisel motion in the soil (*Du et al., 2022; Katinas, Chotěborský, Linda, & Jankauskas, 2019; Kešner et al., 2021; Mak, Chen, & Sadek, 2012; Tamás, Jóri, & Mouazen, 2013; Ucgul, Saunders, & Fielke, 2018)*.

Tsuji's report (*Tsuji et al., 2012*) included several models for cohesion are classified into non-physical, microscopic, and macroscopic models. The latter describes models that are not derived from a micromechanical origin of cohesion, but their formulation is oriented on the macroscopic effect of cohesion. The studies mentioned above about capillary cohesion are examples of the microscopic approach. It is suggested (*Obermayr, Vrettos, Eberhard, & Däuwel, 2014; Tsuji et al., 2012*), to use models derived from macroscopic considerations for practical engineering problems, while the microscopic models may serve for calibration purposes.

Currently, the DEM method is widely used in the study of rocks (*Liu et al., 2022*), soils *(Ding, Song, & Yue, 2022; Dun, Yue, Huang, & Zhang, 2022; Foldager et al., 2022; Gao, Yu, Wang, Li, & Shi, 2022; P. Wang & Yin, 2022; J. Wu, Shen, Yang, & Feng, 2022*), powders, grains *(Guo, Zheng, Zang, & Chen, 2022; M. Wu & Wang, 2022*) or agriculture (*Guo et al., 2022*) because it can adequately describe discrete behaviors of these materials.

The present paper investigates cohesion soil model by Discrete Element Method, considering the pre-stress and the cohesive forces formed by bond bridges among neighboring soil grains. The aim is to explore the evolution of the behavior of soil grains and their relationship with the mechanical properties of cohesive soil.

## MATERIALS AND METHODS

### Discrete element model for cohesive soil

This contribution is focused on the model for cohesive soil. The adhesive force is added to the adhesionless material interaction. For the discrete element model shown here, only forces laws for the contacts between adjacent particles are given. Used software RockyDEM provides all other necessary steps in the simulation, like contact detection, overlaps, and time integration of the particle dynamics and takes care of input and output operations. The description of these steps is omitted here for brevity.

***Normal force model***

The normal force model is described as a hysteretic linear spring model. This model, proposed by Walton & Braun (*Walton & Braun, 1986*), was referred to as the linear hysteresis model. This elastic-plastic (repulsive and dissipative) normal contact model allows simulation of the plastic energy dissipation on contact without introducing the overhead of long simulation time. In addition, since no viscous damping term is used, the energy dissipation is not dependent on the relative velocities of neighboring particles, making the energy dissipation insensitive to other contacts. An additional advantage of this model is that compressible materials can be accurately modeled because the contact forces can be almost zero even at residual overlaps.

$$F_n^t = \begin{cases} min\left(K_{nl} s_n^t, F_n^{t-\Delta t} + K_{nu}\Delta s_n\right) & if\ \Delta s_n \geq 0 \\ max\left( F_n^{t-\Delta t} + K_{nu}\Delta s_n, \lambda K_{nl} s_n^t\right) & if\ \Delta s_n < 0 \end{cases} \tag{1}$$

$$\Delta s_n = s_n^t - s_n^{t-\Delta t} \tag{2}$$

where $F_n^t$ and $F_n^{t-\Delta t}$ are normal elastic-plastic contact forces at the current time $t$ and at previous time $t - \Delta t$, respectively, where $\Delta t$ is the time step, $\Delta s_n$ is the change in the normal contact overlap during the current time. It is assumed positive as particles approach each other and negative when they separate. $s_n^t$ and $s_n^{t-\Delta t}$ are normal overlap values at the current and previous time, respectively. $K_{nl}$ and $K_{nu}$ are the values of loading and unloading contact stiffness, respectively. A typical cycle of loading/unloading is placed in Fig. 1.

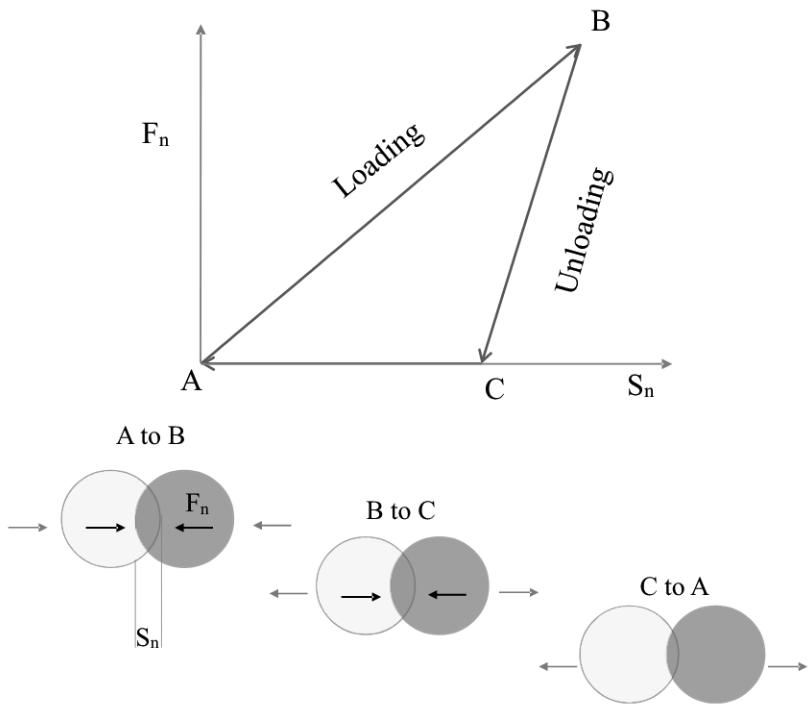


**Fig. 1** Walton & Braun normal contact model.

The loading and unloading stiffnesses are defined by the particle size, the bulk Young's modulus, and the restitution coefficient of contacting materials. The last two are the user inputs into RockyDEM. The coefficient of restitution $\varepsilon$ in Rocky is a measure of energy dissipation for the contacting pair of materials. For the contact of two particles or a particle with a boundary, the loading and unloading equivalent stiffnesses are defined, respectively, as

$$\frac{1}{K_{nl}} = \begin{cases} \frac{1}{K_{nl,p1}} + \frac{1}{K_{nl,p2}} & for\ particle\text{–}\ particle\ contact \\ \frac{1}{K_{nl,p}} + \frac{1}{K_{nl,b}} & for\ particle\text{–}\ boundary\ contact \end{cases} \quad (3)$$

$$K_{nu} = \frac{K_{nl}}{\varepsilon^2} \quad (4)$$

The individual stiffnesses corresponding to a particle and a boundary are computed, respectively, as

$$K_{nl,p} = E_p L \quad (5)$$

$$K_{nl,b} = E_b L \quad (6)$$

where $E_p$ is bulk Young's or elastic modulus of the particle material, $E_b$ is Young's modulus of boundary material, $L$ is the particle size. In long-term contacts, for instance, among particles in a stockpile, the hysteretic linear spring model can give rise to oscillations of very small amplitudes on the normal force and the overlap.

***Tangential force model***

The tangential force model is the linear spring coulomb limit model. In this model, tangential force is elastic-frictional force. If the tangential force were considered purely elastic, the value at time *t* would be:

$$F_{t,e}^{t} = F_t^{t-\Delta t} + K_t \Delta S_t \quad (7)$$

Where $F_t^{t-\Delta t}$ is the value of the tangential force at a previous time, $\Delta S_t$ is the tangential relative displacement of the particles during the timestep, $K_t$ is tangential stiffness (calculated as loading stiffness times tangential stiffness ratio) – this calculation included Young's modulus of particles and their diameter (*Yeom et al., 2019*).

***Adhesive (cohesion) force model***

In the macroscopic scale, cohesive materials are characterized by having shear strength even at minimal confining pressure. It is described by a cohesive intercept ***c*** of the shear strength envelope.

The bond model implemented similar models described in the papers of Gimenez and Potyondy *(Potyondy & Cundall, 2004; Sangrós Giménez, Finke, Nowak, Schilde, & Kwade, 2018*). In this model, a bond is a massless entity of cylindrical shape attached to a pair of neighbor particles that exerts elastic and viscous forces and moments on them as a reaction to deformations caused by their relative motion. If the external load acting on a bond exceeds its specified strength, it will break, and its bonding action over the particles will be the case. The two particles are located at a distance *h* lower than the activation distance given by eq (8)

$$h_{ac} = f_{ac}(r_i + r_j) \quad (8)$$

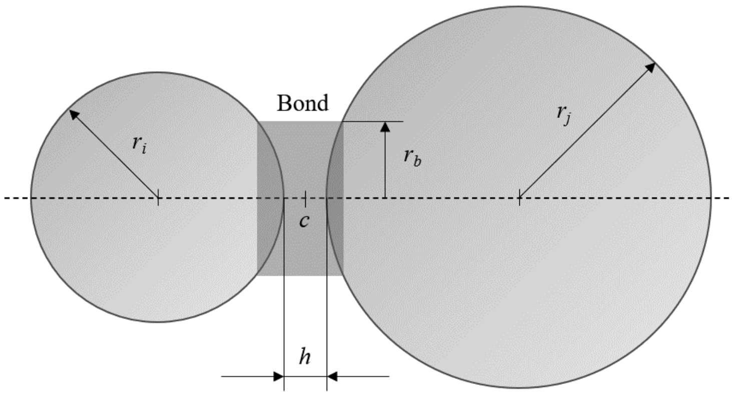


**Fig. 2** Geometry of the bond model between two spherical particles of different sizes

where $r_i$ (m) and $r_j$ (m) are the radii of the bonded particles, as shown in Fig. 2, while $f_{ac}$ (-) is an input parameter as "distance factor". The activation of bonds happens only once at a specific time during a simulation. The radius of the bond between two particles depends only on the radii of those particles

$$r_b = \frac{r_i r_j}{r_i + r_j} \tag{9}$$

The bond model implemented in this module also includes the possibility of adding particle-boundary bonds to the simulation. Those bonds share all characteristics described earlier for particle-particle bonds, except the activation distance, in this case, is given simply by

$$h_{ac} = 2 f_{ac} r_p \tag{10}$$

where $f_{ac}$ is the corresponding "distance factor" and $r_p$ is the radius of the bonded particle. Similarly, the radius of the corresponding bond will be directly $r_b=r_p$ in that case.

At the time of its activation, a bond is undeformed. From that time on, any relative motion of the bonded particles will cause deformation on the bond, to which it will react exerting forces and moments opposing to that relative motion. The bond deformation can be linear or angular, the former caused by both the translational and rotational motion of the bonded particles. At the same time, the latter is only a consequence of their rotational motion. In the module, both types of deformation are calculated incrementally, starting from the time of bond activation, $t_{ac}$. Thus, the linear deformation of a bond at any given time $t$ is provided by

$$s^b = \sum_{t_{ac}}^{t} v_c^{rel} \Delta t \tag{11}$$

where $v_c^{rel}$ is the instantaneous relative velocity at the center point of the bond $c$, while $dt$ is the simulation timestep. The relative velocity $v_c^{rel}$ is calculated as

$$v_c^{rel} = v_i - v_j + \omega_i \times \Delta r_{i-c} - \omega_j \times \Delta r_{j-c} \tag{12}$$

where $v_i$ and $v_j$ are the translational velocities of the bonded particles, $\omega_i$ and $\omega_j$ are the rotational velocities of the bonded particles, $\Delta r_{i\text{-}c}$ is the vector that joints the centroid of the particle $i$ to the bond's center point $c$. The definition is equivalent to the vector $\Delta r_{j\text{-}c}$. The bond in the considered model will oppose the linear deformation $s^b$ by exerting an elastic force on both bonded particles. The normal and tangential components of this force will be given, respectively, by:

$$F_n^b = -K_n^{"} A_b s_n^b \tag{13}$$

$$F_\tau^b = -K_\tau^{"} A_b s_\tau^b \tag{14}$$

where $K_n^{"}$ and $K_\tau^{"}$ are the normal and tangential stiffnesses per unit area, respectively. $A_b$ is the cross-sectional area of the bond, $s_n^b$ and $s_\tau^b$ are the normal and tangential components of the bond's linear deformation $s^b$. The decomposition of the vector $s^b$ is carried out by using the following simple expressions

$$s_n^b = s^b \cdot \hat{n} \tag{15}$$

$$s_\tau^b = s^b - s_n^b \cdot \hat{n} \tag{16}$$

in which $\hat{n}$ is the normal unit vector parallel to the bonds axis.

The breakage criterion is based on the maximum values of the tensile and shear stresses acting on the periphery of the bond. Those values are given, respectively, by

$$\sigma^{max} = -\frac{F_n^b}{A_b} \tag{17}$$

$$\tau^{max} = \frac{|F_\tau^b|}{A_b} \tag{18}$$

During a simulation, the maximum tensile and shear stresses values are constantly monitored for all active bonds. When the tensile strength limit exceeds $\sigma^{max}$ or the shear strength limit exceeds $\tau^{max}$, the bond breaks and, consequently, is deactivated immediately. After such a breakage, a bond cannot be reactivated again during the simulation.

**Tested soil**

The soil tests were conducted in Prague-Suchdol, Czech Republic (50°12'78.51″N, 14°37'58.01″ E). The soil of the experimental field was classified as Haplic Chernozem, including clay (6.52%), sand (29.32%), and silt loam soil (64.16%) (*Kodešová et al., 2016*). The average moisture content was 14.3 wt. %.

## Model calibration

The Rocky DEM software (version 2022R1, ESSS company, Florianopolis, Brazil) was used for the simulation. The NVIDIA Quadro GV100 graphic card was used to operate Rocky DEM software. The DEM analysis and post-processing were performed with an Intel Xeon Gold 6244 (3.6 GHz) computer, 128 GB RAM, and 2x1TB PCIe SSD.

**Tab. 1** Variables setup for cohesive discrete element model

| Material interaction | Normal stiffness (NS) | Normal stress limit (NSL) | Tangential stiffness (TS) | Tangential stress limit (TSL) | Bulk young modulus (YM) |
|---|---|---|---|---|---|
| | $N \cdot m^{-3}$ | kPa | $N \cdot m^{-3}$ | kPa | MPa |
| Particle-particle | $1 \cdot 10^{10}$ | 1000 | $1 \cdot 10^{10}$ | 1000 | 20 |
| | $1 \cdot 10^{9}$ | 500 | $1 \cdot 10^{9}$ | 500 | 40 |
| | $1 \cdot 10^{8}$ | 100 | $1 \cdot 10^{8}$ | 100 | 60 |
| Totally 256 tasks | Static friction 0.7 | | | | |
| | Dynamic friction 0.6 | | | | |
| Particle-boundary | Static friction 0.4 | | | | |
| | Dynamic friction 0.3 | | | | |

A DEM calibration was performed based on a tensile test of the soil (Fig. 3). The tensile test was conducted in the laboratory. Afterward, the value of the soil strength was used in the evaluation model for the DEM tensile test model. The values from the model were compared with those from the experiment. Iterations were compiled for the subsequent model until the course of the curves showed deviations. The setting of the iterations was performed using a DoE approach, and the effects of the DEM parameter's dependency on the cohesive soil properties were determined. The parameters were obtained by optimization of the model results and validated based on the experimental results.

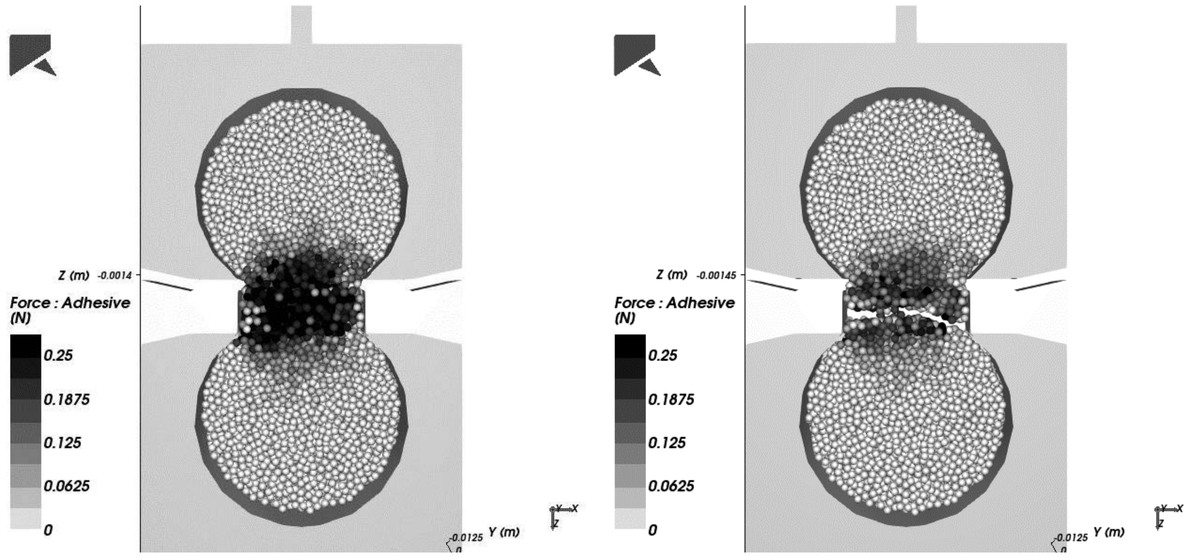


a) b)

c)

**Fig. 3** Tensile test of simulated (a and b) and measured (c) samples. Adhesive force distribution in soil sample before rupture (a) and after that (b) with fracture line.

## RESULTS AND DISCUSSION

The simulated maximal forces and stiffness agreed with experimental data in all cases. A typical comparison is presented in Fig. 4. Simulated maximal forces of the tensile test were within the limits of experimental test values. Power, calculated like area under the tensile curve, seems to show different values, and relationships between simulated and experimental data are too difficult. Because the power is calculated with deformation, the size of discrete elements can probably play a role in the model's accuracy.

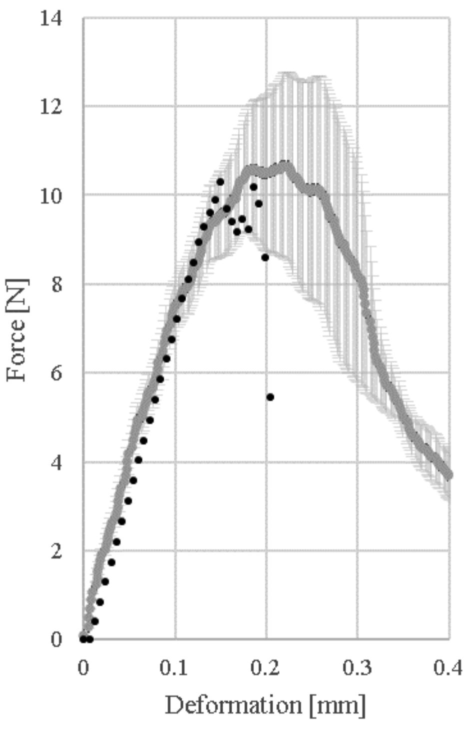


**Fig. 4** Simulated (black) and measured (grey) data from the tensile test, mean and standard deviations are represented by limits.

Good practice models need relative accuracy variables for a simulation setup. The results of the ANOVA multi-criteria analysis of the simulations (Fig. 5) were carried out using the DoE approach. This approach creates a relevant response sensitivity to changes in input variables. In other words, how can the model's input data affect the observed result? The effects analysis shows that the most significant influence on the results of the strength model (maximum strength) has the variable "normal stress limit" and "normal stiffness" and their interaction (Fig. 5a). The model is less influenced by the tangential input parameters. In the case of stiffness, however, the model's sensitivity is also affected by Young's modulus and, after that, by the "tangential stress limit" (Fig. 5c). The energy (Fig. 5b) output cannot be adequately interpreted due to the high error rate compared to the experiments. Still, it seems that it will correlate with the force model and its sensitivity.

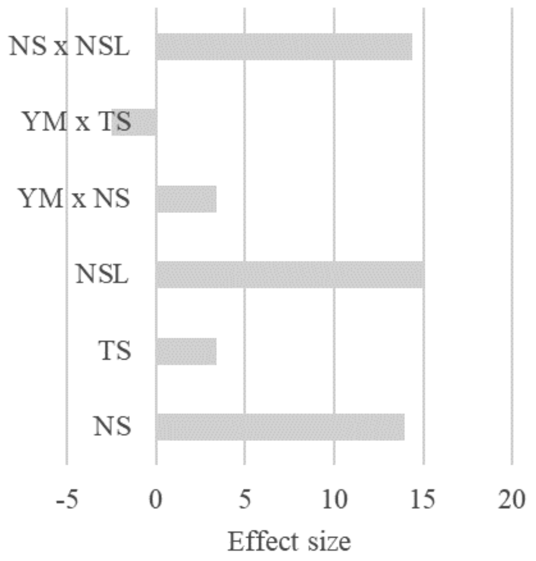


a)

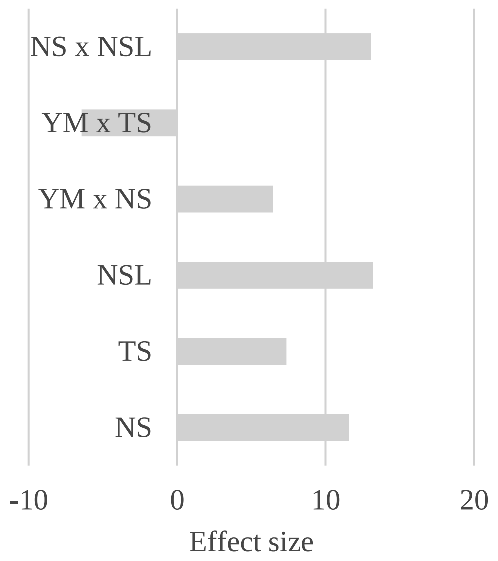


b)

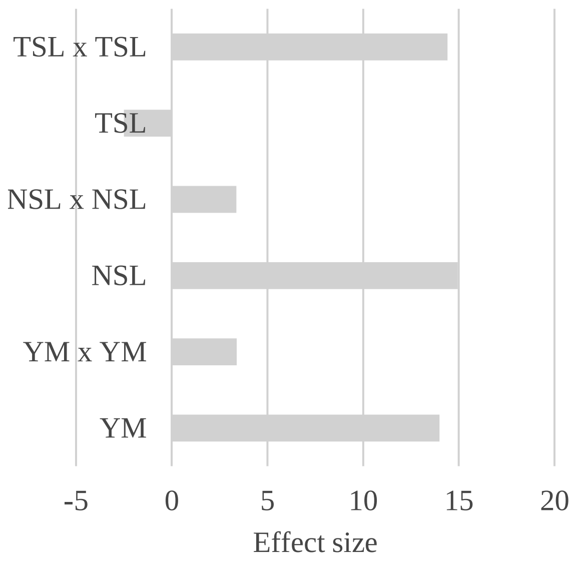


c)

**Fig. 5** Effect of variables (Young's modulus, normal stiffness, normal stress limit, tangential stiffness, tangential stress limit) on responses, (a) – maximal forces, (b) – power, (c) stiffness.

Data from 256 models can be generalized in multivariate linear equations. The results of these statistical models are presented below. The determination index shows a close dependence between the phenomenological model and the simulation results, i.e., the experimentally measured values.

$$F_{max} = 16.3 - 7 \cdot 10^{-5}NS + 7.6 \cdot 10^{-5}TS - 4 \cdot 10^{-9}NSL + 9.5 \cdot 10^{-7}YM \cdot NS - 1.2 \cdot 10^{-6}YM \cdot TS + 1.6 \cdot 10^{-14}NS \cdot NSL$$

$R^2 = 0.93$

$$Power = 9.5 \cdot 10^{-1} - 2.7 \cdot 10^{-5}NS + 2.6 \cdot 10^{-5}TS - 6 \cdot 10^{-10}NSL + 4.2 \cdot 10^{-7}YM \cdot NS - 4.4 \cdot 10^{-7}YM \cdot TS + 2.4 \cdot 10^{-15}NS \cdot NSL$$

$R^2 = 0.94$

$$Stiffness = 16 + 6.2 \cdot 10^{-1}YM - 5.7 \cdot 10^{-3}YM^2 + 2.4 \cdot 10^{-9}NSA - 2.9 \cdot 10^{-20}NSA^2 + 5 \cdot 10^{-9}TSA - 2.2 \cdot 10^{-20}TSA^2$$

$R^2 = 0.99$

The literature does not often describe the cohesive soil model for simulations of agricultural tasks. Most researchers (*Tsuji et al., 2012; X. Wang, Zhang, Huang, & Ji, 2022; Zhang, Zhai, Chen, Zhang, & Huang, 2022)*use cohesionless models or models involving the adhesive properties of discrete elements. Probably one of the reasons is the high sensitivity of the cohesion model to the results of the solution and, therefore, the high demands on the accuracy of the obtained values of the mechanical properties necessary for setting the model. Another disadvantage can be the computational complexity of a model with cohesive properties; compared to a model without cohesion, the computational complexity increases so that the computational time increases up to 10 times. Nevertheless, the cohesive model is more reliable for the soil model within DEM calculations, especially for analyzing the processing of soil and plant residues, than the adhesive or non-cohesive model.

## CONCLUSIONS

The simulations and measurement results show the suitability of using a cohesive soil model for DEM. However, by appropriately setting of cohesion model, it is possible to obtain very accurate output values of the model, which is more suitable for agricultural tasks than the cohesion-less or adhesion models.

## ACKNOWLEDGMENT

This study was supported by the Internal Grant 2020:31200/1312/3109 agency of the Faculty of Engineering, Czech University of Life Sciences in Prague with the name: Model of bulk matter for interaction solution between agriculture tool and soil.

## REFERENCES

1. Asaf, Z., Rubinstein, D., & Shmulevich, I. (2007). Determination of discrete element model parameters required for soil tillage. *Soil and Tillage Research, 92(1–2)*, 227–242.
2. Cundall, P. A., & Hart, R. D. (1992). Numerical modelling of discontinua. *Engineering Computations, 9(2),* 101–113.
3. Ding, F., Song, L., & Yue, F. (2022). Study on Mechanical Properties of Cement-Improved Frozen Soil under Uniaxial Compression Based on Discrete Element Method. *Processes 2022, Vol. 10*, Page 324, 10(2), 324.
4. Du, J., Heng, Y., Zheng, K., Luo, C., Zhu, Y., Zhang, J., & Xia, J. (2022). Investigation of the burial and mixing performance of a rotary tiller using discrete element method. *Soil and Tillage Research, 220*, 105349.
5. Dun, H., Yue, P., Huang, N., & Zhang, J. (2021). Discrete Element Simulation on Sand-Bed Collision Considering Surface Moisture Content. *Processes 2022, Vol. 10*, Page 52, 10(1), 52.
6. Foldager, F. F., Munkholm, L. J., Balling, O., Serban, R., Negrut, D., Heck, R. J., & Green, O. (2022). Modeling soil aggregate fracture

using the discrete element method. *Soil and Tillage Research, 218*, 105295.
7. Gao, Y., Yu, J., Wang, Y., Li, W., & Shi, T. (2022). Breakage effect of calcareous sand on pile tip resistance and the surrounding soil stress. *Energy Reports, 8*, 183–190.
8. Guo, X., Zheng, Z., Zang, M., & Chen, S. (2022). A multi-sphere DE-FE method for traveling analysis of an off-road pneumatic tire on irregular gravel terrain. *Engineering Analysis with Boundary Elements, 139*, 293–312.
9. Katinas, E., Chotěborský, R., Linda, M., & Jankauskas, V. (2019). Wear modelling of soil ripper tine in sand and sandy clay by discrete element method. *Biosystems Engineering, 188*, 305–319.
10. Kešner, A., Chotěborský, R., Linda, M., Hromasová, M., Katinas, E., & Sutanto, H. (2021). Stress distribution on a soil tillage machine frame segment with a chisel shank simulated using discrete element and finite element methods and validate by experiment. *Biosystems Engineering, 209*, 125–138.
11. Kodešová, R., Kočárek, M., Klement, A., Golovko, O., Koba, O., Fér, M., … Grabic, R. (2016). An analysis of the dissipation of pharmaceuticals under thirteen different soil conditions. *Science of The Total Environment, 544*, 369–381.
12. Liu, Z., Li, J., Zhao, Q., Wang, J., Liu, T., & Zhang, Q. (2022). Gradation Design of Phosphorus Tailing–Graded Waste Rock Subgrade Filling Using Discrete Element Method. *Minerals, 12(5)*, 573.
13. Mak, J., Chen, Y., & Sadek, M. A. (2012). Determining parameters of a discrete element model for soil–tool interaction. *Soil and Tillage Research, 118*, 117–122.
14. Mattetti, M., Varani, M., Molari, G., & Morelli, F. (2017). Influence of the speed on soil-pressure over a plough. *Biosystems Engineering, 156*, 136–147.
15. Mouazen, A. M., & Neményi, M. (1999). Finite element analysis of subsoiler cutting in non-homogeneous sandy loam soil. *Soil and Tillage Research, 51(1–2)*, 1–15.
16. Obermayr, M., Vrettos, C., Eberhard, P., & Däuwel, T. (2014). A discrete element model and its experimental validation for the prediction of draft forces in cohesive soil. *Journal of Terramechanics, 53(1)*, 93–104.
17. Potyondy, D. O., & Cundall, P. A. (2004). A bonded-particle model for rock. International *Journal of Rock Mechanics and Mining Sciences, 41(8)*, 1329–1364.
18. Sangrós Giménez, C., Finke, B., Nowak, C., Schilde, C., & Kwade, A. (2018). Structural and mechanical characterization of lithium-ion battery electrodes via DEM simulations. *Advanced Powder Technology, 29(10)*, 2312–2321.
19. Tamás, K., Jóri, I. J., & Mouazen, A. M. (2013). Modelling soil–sweep interaction with discrete element method. *Soil and Tillage Research, 134*, 223–231.
20. Tsuji, T., Nakagawa, Y., Matsumoto, N., Kadono, Y., Takayama, T., & Tanaka, T. (2012). 3-D DEM simulation of cohesive soil-pushing behavior by bulldozer blade. *Journal of Terramechanics, 49(1)*, 37–47.
21. Ucgul, M., Saunders, C., & Fielke, J. M. (2018). Comparison of the discrete element and finite element methods to model the interaction of soil and tool cutting edge. *Biosystems Engineering, 169*, 199–208.
22. Walton, O. R., & Braun, R. L. (1986). Viscosity, granular-temperature, and stress calculations for shearing assemblies of inelastic, frictional disks. *Journal of Rheology, 30(5)*, 949–980.
23. Wang, P., & Yin, Z.-Y. (2022). Effect of particle breakage on the behavior of soil-structure interface under constant normal stiffness condition with DEM. *Computers and Geotechnics, 147*, 104766.
24. Wang, X., Zhang, Q., Huang, Y., & Ji, J. (2022). An efficient method for determining DEM parameters of a loose cohesive soil modelled using hysteretic spring and linear cohesion contact models. *Biosystems Engineering, 215*, 283–294.
25. Wu, J., Shen, Y., Yang, S., & Feng, Z. (2022). Simulation of Track-Soft Soil Interactions Using a Discrete Element Method. *Applied Sciences 2022, Vol. 12*, Page 2524, 12(5), 2524.
26. Wu, M., & Wang, J. (2022). Constitutive modelling of natural sands using a deep learning approach accounting for particle shape effects. *Powder Technology, 404*, 117439.
27. Yeom, S. Bin, Ha, E., Kim, M., Jeong, S. H., Hwang, S. J., & Choi, D. H. (2019). Application of the Discrete Element Method for Manufacturing Process Simulation in the Pharmaceutical Industry. *Pharmaceutics 2019, Vol. 11*, Page 414, 11(8), 414.

28. Zhang, L., Zhai, Y., Chen, J., Zhang, Z., & Huang, S. (2022). Optimization design and performance study of a subsoiler underlying the tea garden subsoiling mechanism based on bionics and EDEM. *Soil and Tillage Research*, *220*, 105375.

**Corresponding author:**

Asc. Prof. Ing., Rostislav Choteborsky, Ph.D., Department of Material Science and Manufacturing Technology, Faculty of Engineering, Czech University of Life Sciences Prague, Kamýcká 129, Praha 6, Prague, 16521, Czech Republic, phone: +420 22438 3274, e-mail: choteborsky@tf.czu.cz